



OPEN

A conical passive magnetic bearing with constant stiffness

R. Bjørk[✉] & C. R. H. Bahl

A nested conical passive magnetic bearing is presented. The bearing consists of a nested conical rotor inside a conical stator, i.e. two coaxial tilted rings of permanent magnets, both with a rectangular cross section. Varying the cone or tilt angle of the rotor and stator we determine the rotor radius that provides the highest force for three different magnetization cases. For this optimal rotor radius, we show that the bearing with the highest volume normalized force also has the highest stiffness, and furthermore often also the highest varying stiffness with axial displacement. Finally, we show that a conical bearings with a tilt angle of 60° has an almost constant stiffness and a linearly varying force with axial displacement, making it ideal as a bearing.

With an increasing focus on energy efficiency, there is a desire to identify and reduce any losses. For rotary machines such losses typically occur as friction at the bearings. Since the development of the strong rare earth based permanent magnets in the 1970'ies and 1980'ies⁵, these materials have been considered for magnetic bearings. The high magnetisation allows for a strong repulsive force between sets of opposing magnets, thus supplying the lift for even heavy rotating parts.

However, as proven by the British mathematician Samuel Earnshaw in 1842¹¹ levitation based on non-dia-magnetic materials can never be stable in all directions, except in cases where the bearing utilizes a gyroscopic effect^{2,28}. Thus, a magnetic bearing based on the repulsion between permanent magnets is inherently unstable. In order to function, some degree of stability is required in the lift (often vertical) direction. This will result in instability in the radial direction and therefore some kind of stabilising, i.e. restoring, force is required in the radial direction. Such a stabilising bearing is referred to as an active magnetic bearing, while the permanent magnet assembly providing the lift is referred to as the passive bearing.

Initial modelling studies of the simplest type of passive magnetic bearing, namely two axially magnetised rings stacked on top of each other was done by Yonnet³⁷. He found that the lifting strength was the same if the rings were radially magnetised. Similar results for the stiffness were later found semi-analytically by Ravaud *et al.*^{26,27} for solid rings of repulsive permanent magnets, and stacks of such systems have also been studied^{33,38}. Closed form expressions for the lift has also been derived analytically^{10,21}. Such systems have also been tested experimentally^{19,25}.

A large number of papers have been published on different passive bearing configurations. The stiffness and lift in different situations have been studied both numerically and experimentally, often with a comparison to models, see e.g. Ref.⁶. To validate the models experimental setups for testing bearings both concentric and off-centre have been presented^{7,24,30,39}. The design with the maximum radial stiffness has been found numerically in Ref.²², by considering the air gap between rotor and stator. Optimally, a bearing configuration should provide both lift and stability, and thus concepts have been suggested with magnet placements attempting to achieve this²⁴. The dynamics of the active bearing has also been investigated^{12,31,32}.

For all passive bearings, it is the stiffness of the radial component that determines the active force needed to keep the bearing stable. A lower negative value of this means a lower force and thus less required energy. However, in all existing studied bearings, the ideal balance between the provided lift and axial stability and the radial instability has not been reached. While bearings with low instability have been realized, the stiffness often varies with axial displacement, making it hard to realize an easily controllable active bearing.

In the current study we analyse a parameterised system designed to supply both lift and stability, by a nested concentric placement of two conical rings. The idea is that if the bearing is shaped like two nested conical rings, with the rotor inside the stator, the magnetic forces will both have a component providing a lifting force along the axis of the bearing, but also a component along the radial direction, which might allow the stiffness along this direction to be designed as desired.

The properties of a conically nested passive magnetic bearing have not previously been considered in literature. The properties of a number of concentric bearings stacked in a cone-shape has been considered¹, but here

Department of Energy Conversion and Storage, Technical University of Denmark - DTU, Anker Engelunds Vej, DK-2800 Kgs, Lyngby, Denmark. ✉email: rabj@dtu.dk

the tilting of the concentric magnetic rings were not considered, i.e. the bearing was not truly cone-shaped. A number of cone-shaped active magnetic bearings have been considered^{13,18,20}, including complex structures with cone-shaped teeth³⁵ and bearing for use in magnetically suspended flywheels^{9,34}. However, all of these works considers the dynamics of the active bearing and not the properties of a nested conical passive bearing.

The bearing investigated here is a passive bearing and will thus always be unstable in one direction, as per Earnshaws theorem, ignoring dynamic effects. The bearing will thus have to be stabilized by an active magnetic bearing, as is always the case for a passive magnetic bearing¹⁹.

Here the forces in the nested conical bearing are found through modelling using the finite element framework Comsol Multiphysics, which is applicable as the bearing is axi-symmetric. This means that the modelling can be performed at high resolution. A modeling approach is justified, as the bearing modelled is a fully magnetostatic system for which simulated magnetic fields are known to fully reproduce experimentally measured fields, see e.g. Refs. 4,8,14,16,23,29. The specific model used here has previously been used to calculate the force of passive magnetic bearings and compared with experiments with good agreement²⁴. For these reasons, the results of the modeling work presented here are directly applicable to practical real-world passive magnetic bearings.

Physics

We consider an axi-symmetric bearing which provides a force in the z -direction, F_z , which we also denote as the “lift”. Besides its lift, a bearing is also characterized by its stiffness, \mathbf{K} , which is the negative of the derivative of the force in a specific direction with respect to the displacement in the same direction, i.e.

$$\begin{aligned}\mathbf{K} &= - \left(\frac{dF_x}{dx} \hat{x} + \frac{dF_y}{dy} \hat{y} + \frac{dF_z}{dz} \hat{z} \right) \\ &= - (K_x \hat{x} + K_y \hat{y} + K_z \hat{z}).\end{aligned}\quad (1)$$

The fact that passive magnetic levitation is not possible is summed up in Earnshaw’s theorem¹¹, which states that the sum of the three stiffness components is equal to zero. Here we consider a bearing with a radial symmetry where thus $K_x = K_y = K_r$. This means that the radial stiffness in the following can be calculated from the stiffness in the z -direction as

$$K_r = -\frac{1}{2}K_z. \quad (2)$$

as long as the bearing is axi-symmetric.

To determine the force and stiffness of the bearing considered, we have realized a magnetostatic finite element (FEM) axi-symmetric model of the bearing in Comsol Multiphysics. The equation solved in the FEM framework is the magnetic scalar potential equation

$$-\nabla \cdot (\mu_0 \mu_r \nabla V_m) = 0. \quad (3)$$

Here μ_0 is the permeability of free space, μ_r is the relative permeability, which is assumed to be constant and isotropic, and V_m is the magnetic scalar potential. The magnetic field is then calculated as $-\nabla V_m = \mathbf{H}$.

To determine the force on either the stator or the rotor, Maxwell’s stress tensor, \mathbb{T} , must be integrated across the surface covering either of these¹¹

$$\mathbf{F} = \oint_{S'} \mathbb{T} \cdot d\mathbf{a} \quad (4)$$

where S' denotes the closed surface surrounding one of the two bearing parts and $d\mathbf{a}$ is an area element of this. With no electrical fields, Maxwell’s stress tensor is given by

$$T_{ij} = \frac{1}{\mu_0} \left(B_i B_j - \frac{1}{2} \delta_{ij} B^2 \right), \quad (5)$$

where $\mathbf{B} = (B_x, B_y, B_z)$ is the magnetic flux density. This integration is automatically done in the Comsol framework.

As both the rotor and stator are axi-symmetric, there is no angular dependence on the force. This also means that the force on the rotor will be the same regardless of the rotation speed of the rotor.

The built-in Comsol Multiphysics solver *GMRES*, which is a Generalized Minimum RESidual iterative method solver, is used to solve Eq. (3) on the finite element mesh. The computational volume is chosen large enough that the boundaries of the simulation volume do not affect the calculations and a fine enough mesh is chosen that the results are verified not to vary when further increasing the mesh size. As we consider an axi-symmetric model, the simulations are 2D, and a very high mesh resolution can be used, eliminating the known convergence issues with bearing finite element models in 3D⁶. As the system modelled is a magnetostatic system, the finite element modeling approach is known to fully reproduce the field created by experimental setups. Therefore a pure modeling is justified.

Bearing geometry

We consider a bearing consisting of nested conical axi-symmetric magnet rings with a quadratic, i.e. square, cross-section. This bearing concept is illustrated in Fig. 1 and can be said to resembles two nested magnetic “bowls”. We consider a design where the stator is larger than the rotor, i.e. the rotor is nested inside the stator.

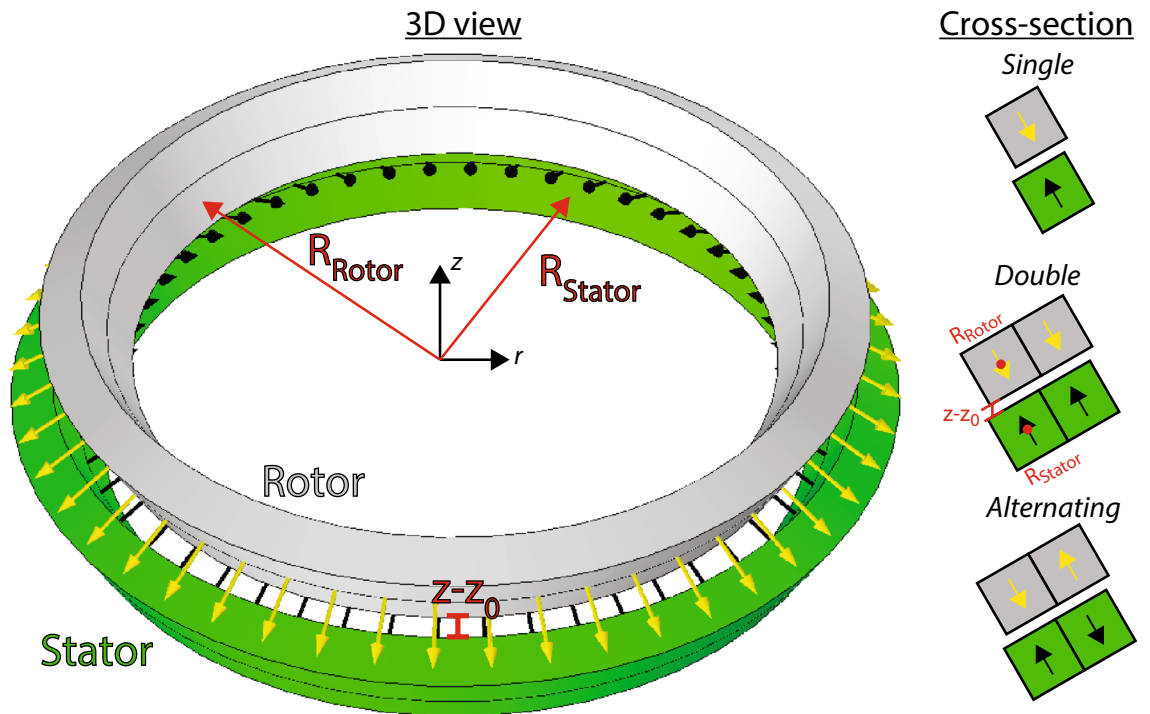


Figure 1. The bearing geometry considered. The stator, shown in green, and the rotor, shown in grey, each consists of two tilted rings of permanent magnets with a quadratic cross-section. The rotor has an inwards magnetization normal to the surface of the rings, while the stator has an outwards magnetization, as indicated by the arrows. The radii R_{rotor} and R_{stator} , which are the radius to the center of the lower ring in either, is also indicated, as is $z - z_0$. The rotor is displaced along the z -axis. The bearing illustrated here has a tilt angle of 30° , as also illustrated in Fig. 2. On the right is shown a cross-section of the bearing, with the three types of magnet configurations considered, as explained in the text. The geometry illustrated on the left is the double bearing.

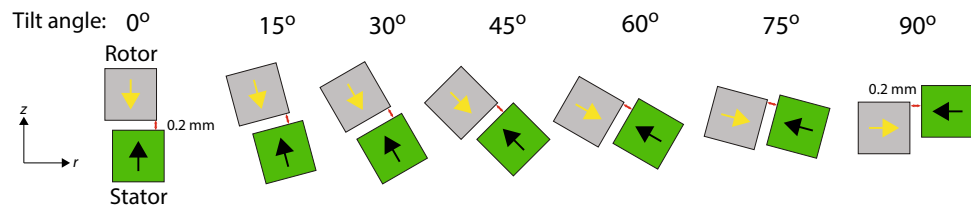


Figure 2. A cross-section of the bearing for the different tilt angles of the rings. The black and yellow arrows indicated the direction of magnetization of the rotor and stator, respectively. Shown as a red line is the minimum distance between the rotor and the stator in each configuration, which is always 0.2 mm.

The rotor and stator are centered on the same axis, and when load is applied on the rotor bearing this will move along the z -axis. The stator has a magnetization direction that is along the inwards normal to its surface, while the rotor has an outwards magnetization direction normal to its surface. Thus, there is repulsion between the rings. Switching both magnetization directions results in an identical situation. It is noted that while producing such tilted conical rings of permanent magnets can be difficult if the rings are to be one piece, the rings can easily be made of cubes of permanent magnets placed in a ring, similar to Ref.²⁴.

In order to ensure that there is always a clearance between the rotor and the stator, we define the value of z_0 to be the z -value at which the stator and rotor have a minimum distance between them of 0.2 mm as shown in Fig. 2. The conical rings that make up both the rotor and the stator have quadratic cross-section side lengths of 3 mm. The radius of the center of the tilted ring in the stator is fixed at 24 mm, while it is varied for the rotor. As shown in Fig. 2 we consider different tilt angles of the stator and rotor rings in the bearing, and these are always tilted by the same angle. The tilt angle is varied continuously, and as the magnetization is always normal to the surface of the magnets to allow for use a standard cube magnets, the passive bearing will at a tilt angle of 90° end up being a repulsive-type radially magnetized bearing³⁸.

We also consider extended ring geometries, with twice the cross-section and different magnetization directions, as shown in Fig. 1, where the rotor and stator radii are also indicated. The variation of cross-section is

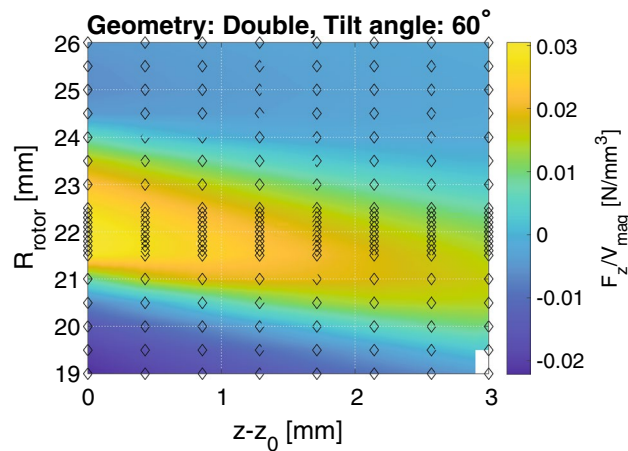


Figure 3. A surface map of the volume normalized force, F_z/V_{mag} , as function of the radius of the rotor and the relative z -displacement for the bearing with a double geometry and a tilt angle of 60° . The diamonds show the data points used to interpolate the surface. Note that $z - z_0$ is a function of R_{rotor} and thus the absolute z -position of the rotor increase as the rotor radius increases. At high values of R_{rotor} the rotor is entirely above the stator.

done because the ratio of the magnets' dimensions (cross-sectional width or height) to the length of the air-gap is known to have a major influence on the bearing stiffness¹⁷. The three different magnetization directions considered are the single bearing, which consists of two tilted concentric rings with opposite magnetization, the double bearing which is similar to the single bearing, except with two magnets in each tilted ring, and finally the alternating bearing is similar to the double bearing, except that the magnetization of one part of the magnet is reversed in both the stator and rotor rings. We assume that the permanent magnets in the bearing have a remanence of 1.4 T and a relative permeability of $\mu_r = 1$, which is very close to the typical experimental values for NdFeB magnets¹⁵.

Results

All results presented in this manuscript are directly available from the data repository in Ref.³.

Initially, a variation study was conducted to determine the optimal geometry of a bearing as function of the tilt angle and the bearing type. Tilt angles from 0° to 90° in steps of 15° were considered. Combined with the three bearing types studied, this gives a total of 21 bearings modelled.

For each of these 21 bearings the radius of the rotor, R_{rotor} , was varied from 19 mm to a value such that the minimum separation was 0.2 mm between the stator and the rotor in steps of 0.5 mm and the relative z -position, $z - z_0$ in 8 steps from 0 to 3 mm. For a tilt angle of 0° where the gap is always at least 0.2 mm, the maximum R_{rotor} was 26 mm. It is noted that at $z - z_0 = 0$ mm the minimum distance between the rotor and the stator is 0.2 mm. This makes z_0 a function of R_{rotor} , i.e. the rotor radius can be larger than the stator radius, as long as the rotor is vertically positioned higher than the stator. The $z - z_0 = 0$ mm ensures that the minimum distance between the rotor and the stator is always kept and that these never overlap.

When the rotor radius is varied the volume of it changes. To account for this, in the following we consider the force in the z -direction normalized with respect to the total volume of the magnet rings in both the stator and the rotor.

An adaptive routine is used to determine the optimal rotor radius to a precision of 0.1 mm. First, the volume normalized force was computed in steps of 0.5 mm for R_{rotor} , and afterwards with 0.1 mm steps between the three highest values at $z - z_0 = 0$ mm. Figure 3 illustrates this by showing the volume normalized force, F_z/V_{mag} , as a function of the rotor radius and the $z - z_0$ -displacement of the rotor for a bearing with a double geometry and a tilt angle of 60° .

For all bearings the value of R_{rotor} where the volume normalized force is largest at $z - z_0 = 0$ mm are shown in Fig. 4, i.e. for the different tilt angles and bearing configurations. To compute these values, it is not necessary to perform a variation in z , i.e. calculate values different from $z - z_0 = 0$ mm, but this is nevertheless done in Fig. 3 to acquire an understanding of the variation of the bearing with $z - z_0$ for all values of R_{rotor} . As can be seen from Fig. 4 the optimal value of R_{rotor} is almost identical for the different bearing geometries considered, with decreasing rotor radius for increasing tilt angle, as expected. The maximum force are also shown at the optimal value of R_{rotor} in Fig. 4.

For each for the optimal R_{rotor} values the volume normalized force was computed at $z - z_0$ values from 0 to 3 mm in 80 steps to obtain a high resolution data set. The results are shown in Fig. 5. As can be seen from the figure, the alternating bearing has the largest volume normalized force, followed by the single bearing and finally the double bearing, regardless of tilt angle. This clearly shows that for the tilted bearing considered here, adding additional rings of permanent magnet, as is the case going from the single to the double bearing, does not result

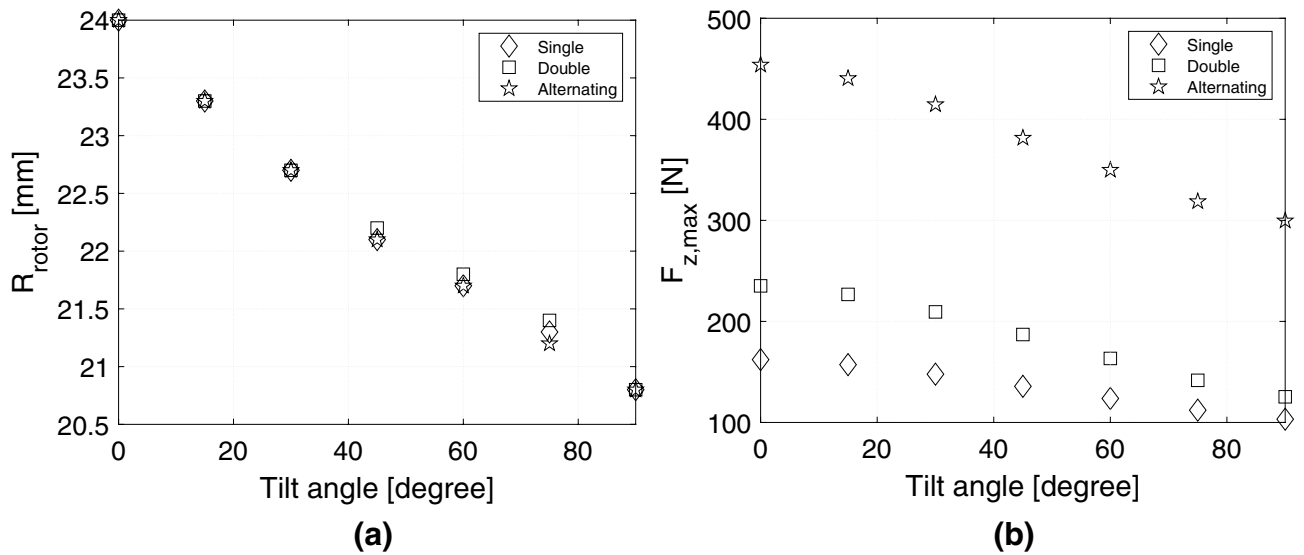


Figure 4. (a) The rotor radius, R_{rotor} , at which the volume normalized force, F_z/V_{mag} , at $z - z_0 = 0$ mm is largest, (b) the largest force at the optimal rotor radius, for the different bearing geometries and tilt angles considered.

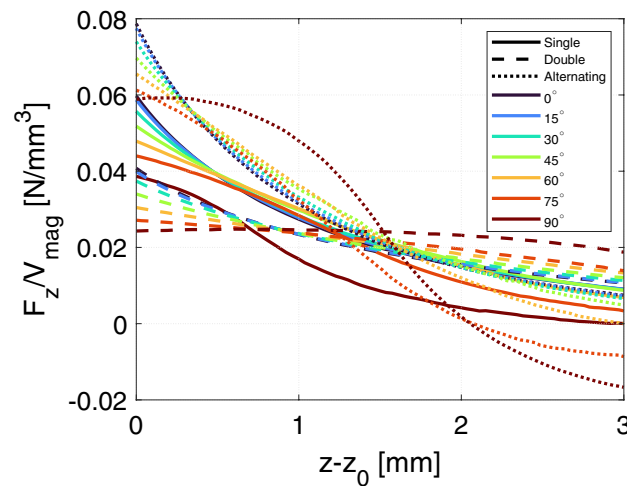


Figure 5. The volume normalized force in the z -direction as function of the relative displacement in the z -direction for the different bearings considered.

in a gain in volume normalized force. However, if one part of the ring is flipped, it can be an advantage. For all configurations the larger the tilt angle, the lower the volume normalized force.

Notice that for high $z - z_0$ values the force can become negative for the Alternating geometry. This is because the magnets in this geometry have opposite magnetization direction and at such a high $z - z_0$ the configuration is such that the rotor and stator magnets attract each other.

For each volume normalized force curve, we fitted a double exponential function of the form $F_z/V_{mag} = ae^{b(z-z_0)} + ce^{d(z-z_0)}$ and from this fit calculated the stiffness, K_z , as the derivative with respect to z . This was done to smooth out small numerical variations in the force calculations, which can lead to large variations in the computed stiffness. The volume normalized stiffness in the z -direction is shown in Fig. 6. The r -direction stiffness can be calculated using Eq. (2) but is not shown due to brevity. The results follow the same trend as the volume normalized force shown in Fig. 5, i.e. that the lower tilt angles result in the largest absolute stiffness, and that the alternating design is the type with the largest absolute stiffness.

We can also directly compare the force provided by the bearing and the axial stiffness of the bearing. Shown in Fig. 7 is the ratio of the axial force provided by the bearing to its axial stiffness. As can be seen from the figure, the double bearing generally has the highest ratio. Interestingly the trend as a function of tilt angle changes as a function of relative z -displacement, with the high tilt angles having the highest ratio at lowest relative z -displacement, but the lowest ratio at high displacements.

Typically the desired properties of a bearing are that it provides a high amount of lift at a relative low absolute stiffness, such that the required force from the active bearing is as small as possible. Of course a relative low

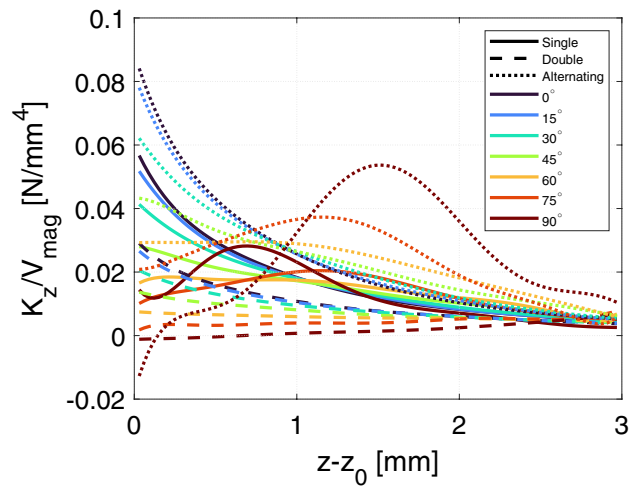


Figure 6. The volume normalized stiffness in the z -direction as function of the relative z -displacement for the different bearings considered. The stiffness in the r -direction can simply be calculated according to Eq. (2).

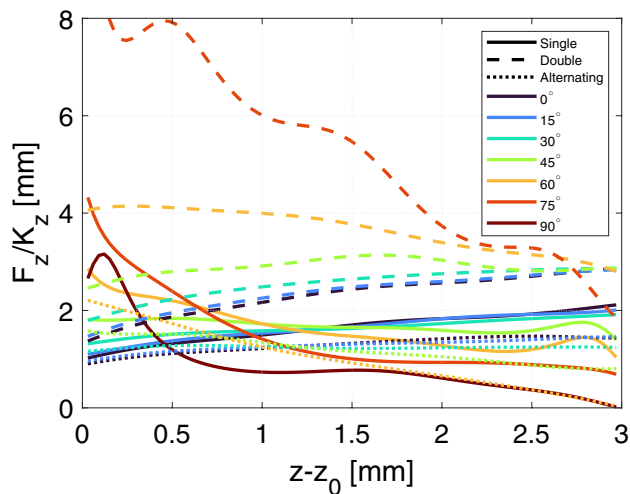


Figure 7. The ratio of the axial force of the bearing to its axial stiffness, as a function of the relative z -displacement for the different bearings considered.

stiffness will mean a high displacement with varying load, so the choice of stiffness is always a compromise. An initial idea to improve the performance of the bearing is to scale it up. As the magnetic field scales with the geometry of the bearing, the absolute lift of the bearing will increase as the size of the bearing is increased. However, the relative stiffness, which is the gradient of the force with respect to the size of the bearing remains constant.

This argument shows that scaling the bearing can be used to provide more lift, but it does not change the stiffness of the bearing. Therefore it is crucial to consider more in-depth the stability of the bearings simulated here. Considering this, we determine the bearing which would be easiest to control by an active bearing over the z -range considered here. This would be a bearing that has a constant K_z -value in the z -range considered, but which also provides a high force over this range. This can be investigated by considering the relative standard deviation, σ/μ , i.e. the standard deviation, σ , divided by the mean, μ , for both the force and stiffness over the z -range considered. This is shown in Fig. 8 for all bearings which have $K_z > 0$ over the z -range considered, i.e. which are stable in the z -direction. It is noted that μ now denotes the mean, and is not to be confused with its earlier usage as the relative permeability.

Choosing the best bearing from Fig. 8 depends on the desired characteristics of the bearing. If one desired a bearing that is easy to control, i.e. has a mostly constant stiffness, the double geometry with a tilt angle between 60° – 75° is clearly the best. However, as shown in Fig. 5 this bearing also provides the lowest lift of the bearings considered. Depending on the active bearing used to stabilize the passive bearing, it is possible that it was the maximum negative stiffness in the movement range considered that was important to dimension the active bearing. In this case passive bearings with a tilt angle of 45° seem to provide a good compromise between lift and stiffness.

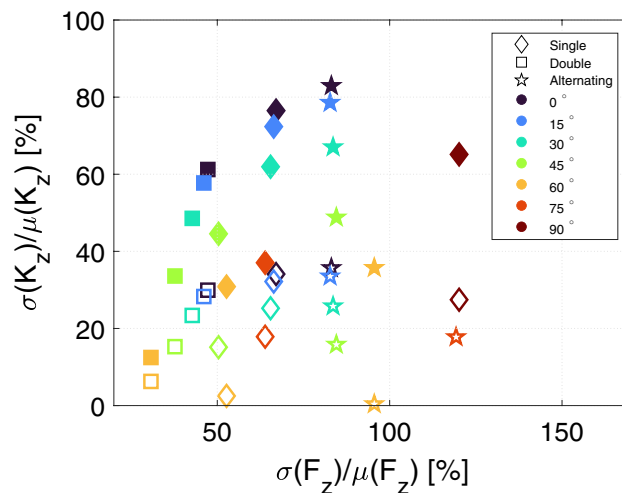


Figure 8. The relative standard deviation of the stiffness in the z -direction in percent as function of the relative standard deviation of the force in the z -direction in percent. The filled symbols consider the full $z - z_0$ -range from 0 to 3 mm, while the unfilled symbols consider only the $z - z_0$ -range from 0 to 1 mm. Only bearings which are stable in the z -direction, i.e. have $K_z > 0$ over the z -range considered, are shown.

When a smaller $z - z_0$ range of 1 mm is considered, all bearings with a tilt angle of 60° display almost constant stiffness as a function of displacement. This is a remarkable property, as such a bearing is very easy to control with an active bearing. Furthermore, the alternating bearing with a tilt angle of 60° has a high value of $\sigma(F_z)/\mu(F_z)$, which means that it has a linear variation in z , with a large force at $z - z_0 = 0$ mm and a low force at $z - z_0 = 1$ mm. This is actually an ideal bearing, as the exact load on the rotor is not of importance, as long as it is between the minimum and maximum lift, and at the same time the stiffness is constant regardless of the load.

It is noted that the 0° and 90° for the single and double configurations is similar to the classical bearing geometry presented in Refs.^{21,26,36,37}. Indeed, the 0° has the highest relative force. The range of the relative stiffness, however, is larger, allowing more freedom in the design. Thus, by varying the tilt angle and the bearing geometry it is possible to tailor a bearing to the desired characteristics.

Potential improvements

Additional methods to improve the force and stiffness of the presented bearings may also be considered. One option is to consider the shape and also exact magnetization direction of the two opposing rings in the single configuration. Only the doubling in one direction has been studied here, but other changes could be considered. Varying the exact direction of the magnetization in the rings could also be explored, to see if better configurations could be determined. Another option could be to look at closing the flux loop on the “back” side of both the rotor and stator rings in the alternating design with iron pieces. Previously, this has been shown to increase the stiffness and lift in a magnetic bearing²⁴.

Finally, we remark that the conical bearing could also be reversed, such that the bearing provided an attractive force. In this configuration it could be used in an “upside-down” configuration to compensate gravity on the rotor by supplying a pull instead of a lift.

Conclusion

We presented a concentric magnetic bearing consisting of two coaxial nested concentric rings of opposing permanent magnets as the rotor and stator. Both magnet rings had a rectangular cross-section. We examined three different configurations, and determined the rotor radius that provided the highest force as a function of the tilt angles of the stator and rotor rings.

For this optimal rotor radius, we showed that the bearing with the highest force also has the highest stiffness, and furthermore often also the highest variation in stiffness with axial displacement. Over a 1 mm displacement in z , a bearing with a tilt angle of 60° has a constant stiffness and a linearly varying force, meaning that it can support a large variety of loads, making it the ideal bearing.

Data availability

All data presented in this manuscript are directly available from Ref.³. The simulation files are each typically ~ 10 Gb and are available upon request from the corresponding author.

Received: 4 October 2021; Accepted: 24 February 2022

Published online: 08 March 2022

References

- Bassani, R. & Villani, S. Passive magnetic bearings: the conic-shaped bearing. *Proc. Inst. Mech. Eng. J. Tribol.* **213**(2), 151–161 (1999).
- Berry, M. V. The levitron™: an adiabatic trap for spins. *Proc. Roy. Soc. Lond. Ser. A Math. Phys. Eng. Sci.* **452**(1948), 1207–1220 (1996).
- Björk, R., & Bahl, C.R.H. Data set for “a conical passive magnetic bearing with constant stiffness”. <https://doi.org/10.11583/DTU.13251359> (2020).
- Björk, R., Bahl, C. R. H., Smith, A., Christensen, D. & Pryds, N. An optimized magnet for magnetic refrigeration. *J. Magn. Magn. Mater.* **322**(21), 3324–3328 (2010).
- Coey, J. Hard magnetic materials: a perspective. *IEEE Trans. Magn.* **47**(12), 4671–4681 (2011).
- Dagnæs-Hansen, N. A. & Santos, I. F. Permanent magnet thrust bearings for flywheel energy storage systems: analytical, numerical, and experimental comparisons. *Proc. Inst. Mech. Eng. C J. Mech. Eng. Sci.* **233**(15), 5280–5293 (2019).
- Detoni, J. Progress on electrodynamic passive magnetic bearings for rotor levitation. *Proc. Inst. Mech. Eng. C J. Mech. Eng. Sci.* **228**(10), 1829–1844 (2014).
- Eriksen, D. *et al.* Design and experimental tests of a rotary active magnetic regenerator prototype. *Int. J. Refrig.* **58**, 14–21 (2015).
- Fang, J., Wang, C. & Tang, J. Modeling and analysis of a novel conical magnetic bearing for vernier-gimballing magnetically suspended flywheel. *Proc. Inst. Mech. Eng. C J. Mech. Eng. Sci.* **228**(13), 2416–2425 (2014).
- Furlani, E. A formula for the levitation force between magnetic disks. *IEEE Trans. Magn.* **29**(6), 4165–4169 (1993).
- Griffiths, D. J. *Introduction to electrodynamics* (Pearson Education, London, 2014).
- Hegazy, U. & Amer, Y. A time-varying stiffness rotor-active magnetic bearings system under parametric excitation. *Proc. Inst. Mech. Eng. C J. Mech. Eng. Sci.* **222**(3), 447–458 (2008).
- Jing, Y., Lie, Y. & Jing, X. Coupled dynamics and control of a rotor-conical magnetic bearing system. *Proc. Inst. Mech. Eng. J. Tribol.* **220**(7), 581–586 (2006).
- Karimi, P., Khodadadi Darban, A. & Mansourpour, Z. A finite element model to simulate magnetic field distribution and laboratory studies in wet low-intensity magnetic separator. *J. Min. Environ.* **10**(3), 717–727 (2019).
- Katter, M. Angular dependence of the demagnetization stability of sintered nd-fe-b magnets. *IEEE Trans. Magn.* **41**(10), 3853–3855 (2005).
- Kennedy, M. W., Akhtar, S., Bakken, J. A. & Aune, R. E. Analytical and experimental validation of electromagnetic simulations using comsol®, re inductance, induction heating and magnetic fields. In: COMSOL Users Conference, Stuttgart Germany. pp. 1–9 (2011).
- Lang, M. & Fremerey, J. Optimization of permanent-magnet bearings. In: Proceedings of the 6th international symposium on magnetic suspension technology. pp. 111–116 (2001).
- Lee, C.-W. & Jeong, H.-S. Dynamic modeling and optimal control of cone-shaped active magnetic bearing systems. *Control. Eng. Pract.* **4**(10), 1393–1403 (1996).
- LeMarquand, G. & Yonnet, J.-P. A partially passive magnetic suspension for a discoidal wheel. *J. Appl. Phys.* **64**(10), 5997–5999 (1988).
- Lin, L.-C. & Gau, T.-B. Feedback linearization and fuzzy control for conical magnetic bearings. *IEEE Trans. Control Syst. Technol.* **5**(4), 417–426 (1997).
- Marth, E., Jungmayr, G. & Amrhein, W. A 2-d-based analytical method for calculating permanent magnetic ring bearings with arbitrary magnetization and its application to optimal bearing design. *IEEE Trans. Magn.* **50**(5), 1–8 (2013).
- Moser, R., Sandtner, J. & Bleuler, H. Optimization of repulsive passive magnetic bearings. *IEEE Trans. Magn.* **42**(8), 2038–2042 (2006).
- Nakata, T. & Fujiwara, K. Summary of results for benchmark problem 13 (3-d nonlinear magnetostatic model). COMPEL-The International Journal for Computation and Mathematics in Electrical and Electronic Engineering (1992).
- Nielsen, K. K., Bahl, C. R. H., Dagnæs, N. A., Santos, I. F. & Björk, R. A passive permanent magnetic bearing with increased axial lift relative to radial stiffness. *IEEE Trans. Magn.* <https://doi.org/10.1109/TMAG.2020.3042957> (2020).
- Ohji, T., Mukhopadhyay, S., Iwahara, M. & Yamada, S. Permanent magnet bearings for horizontal-and vertical-shaft machines: a comparative study. *J. Appl. Phys.* **85**(8), 4648–4650 (1999).
- Ravaud, R., Lemarquand, G. & Lemarquand, V. Force and stiffness of passive magnetic bearings using permanent magnets. Part 1: Axial magnetization. *IEEE Trans. Magn.* **45**(9), 3334–3342 (2009).
- Ravaud, R., Lemarquand, G. & Lemarquand, V. Force and stiffness of passive magnetic bearings using permanent magnets. Part 2: Radial magnetization. *IEEE Trans. Magn.* **45**(7), 2996–3002 (2009).
- Simon, M. D., Heflinger, L. O. & Ridgway, S. Spin stabilized magnetic levitation. *Am. J. Phys.* **65**(4), 286–292 (1997).
- Siyambalapitiya, C. S. Model and validation of static and dynamic behavior of passive diamagnetic levitation for energy harvesting (2012).
- Sun, J., Chen, D. & Ren, Y. Stiffness measurement method of repulsive passive magnetic bearing in sgmscmg. *IEEE Trans. Instrum. Meas.* **62**(11), 2960–2965 (2013).
- Sun, J., Zhou, H. & Ju, Z. Dynamic stiffness analysis and measurement of radial active magnetic bearing in magnetically suspended molecular pump. *Sci. Rep.* **10**(1), 1–16 (2020).
- Tsai, N., Li, H., Lin, C., Chiang, C. & Wang, P. Magnetic damping and stiffness effects on rod translation by active magnetic bearing. *Proc. Inst. Mech. Eng. C J. Mech. Eng. Sci.* **225**(8), 1950–1962 (2011).
- Van Beneden, M., Kluyskens, V. & Dehez, B. Optimal sizing and comparison of permanent magnet thrust bearings. *IEEE Trans. Magn.* **53**(2), 1–10 (2016).
- Xiang, B. & Tang, J. Suspension and titling of vernier-gimballing magnetically suspended flywheel with conical magnetic bearing and lorentz magnetic bearing. *Mechatronics* **28**, 46–54 (2015).
- Xu, S. & Fang, J. A novel conical active magnetic bearing with claw structure. *IEEE Trans. Magn.* **50**(5), 1–8 (2013).
- Yonnet, J. P. Passive magnetic bearings with permanent magnets. *Intermag. (Int. Magn.) Conf. MAG* **14**(5), 803–805 (1978).
- Yonnet, J. P. Permanent magnet bearings and couplings. *IEEE Trans. Magn.* **17**(1), 1169–1173 (1981).
- Yonnet, J.-P., Lemarquand, G., Hemmerlin, S. & Olivier-Rulliere, E. Stacked structures of passive magnetic bearings. *J. Appl. Phys.* **70**(10), 6633–6635 (1991).
- Zhang, L., Wu, H., Li, P., Hu, Y., & Song, C. Design, analysis, and experiment of multiring permanent magnet bearings by means of equally distributed sequences based monte carlo method. *Math. Prob. Eng.* 2019 (2019).

Acknowledgements

This work was financed by the Energy Technology Development and Demonstration Program (EUDP) under the Danish Energy Agency, project no. 64016-0058. The authors wishes to thank Dr. Kaspar Kirstein Nielsen for fruitful discussions on the bearing design.

Author contribution

R.B. and C.B. designed the bearing studied, R.B. performed the numerical simulation, and R.B. and C.B. wrote the manuscript text while R.B. prepared all figures. All authors reviewed the manuscript.

Competing interest

The authors declare no competing interests.

Additional information

Correspondence and requests for materials should be addressed to R.B.

Reprints and permissions information is available at www.nature.com/reprints.

Publisher's note Springer Nature remains neutral with regard to jurisdictional claims in published maps and institutional affiliations.



Open Access This article is licensed under a Creative Commons Attribution 4.0 International License, which permits use, sharing, adaptation, distribution and reproduction in any medium or format, as long as you give appropriate credit to the original author(s) and the source, provide a link to the Creative Commons licence, and indicate if changes were made. The images or other third party material in this article are included in the article's Creative Commons licence, unless indicated otherwise in a credit line to the material. If material is not included in the article's Creative Commons licence and your intended use is not permitted by statutory regulation or exceeds the permitted use, you will need to obtain permission directly from the copyright holder. To view a copy of this licence, visit <http://creativecommons.org/licenses/by/4.0/>.

© The Author(s) 2022